Cyan Fluorescent Protein: Molecular Dynamics, Simulations, and Electronic Absorption Spectrum

Isabelle Demachy, Jacqueline Ridard,* Hélène Laguitton-Pasquier, Elodie Durnerin, Germain Vallverdu, Pierre Archirel, and Bernard Lévy

Laboratoire de Chimie Physique, UMR 8000 CNRS-Université de Paris-Sud, 91405 Orsay Cedex, France

Received: August 18, 2005; In Final Form: October 4, 2005

The dynamics and electronic absorption spectrum of enhanced cyan fluorescent protein (ECFP), a mutant of green fluorescent protein (GFP), have been studied by means of a 1 ns molecular dynamics (MD) simulation. The two X-ray conformations A′ and B′ of ECFP were considered. The chromophore was assumed to be neutral, and all titratable residues were taken in their standard protonation state at neutral pH. The protein was embedded in a box of water molecules (and counterions). The first result is that the two conformations A′ and B′ are found to be stable all along the simulation. Then, an analysis of the hydrogen-bond networks shows strong differences between the two conformations in the surroundings of the nitrogen atom of the indolic part of the chromophore. This is partly due to the imperfection in the β barrel near the His148 residue, which allows the access of one solvent molecule inside the protein in conformation A′. Finally, quantum mechanical calculations of the electronic transition energies of the chromophore in the charge cloud of the protein and solvent water molecules were performed using the TDDFT method on 160 snapshots extracted every 5 ps of the MD trajectories. It is found that conformations A′ and B′ exhibit very similar spectra despite different H-bond networks involving the chromophore. This similarity is related to the weak charge transfer involved in the electronic transition and the weak electrostatic field created by ECFP near the chromophore, within the hypotheses made in the present simulation.

1. Introduction

Fluorescent proteins, mainly green fluorescent protein (GFP) and its parents, are efficient markers for gene expression, cellular localization of proteins, and various dynamic intracellular events.[1,2] In particular, GFP has largely contributed to the development of imaging methods in cell biology during past decades. A great number of mutants have been generated by mutagenesis to obtain specific photophysical properties such as red- or blue-shifted emissions[3]. Some of the GFP variants, enhanced cyan fluorescent protein (ECFP) and yellow fluorescent protein (YFP), are currently used to form a donor−acceptor couple in resonance energy transfer technics (FRET) employed in living cells to characterize protein interactions or conformational changes.[4]

A huge amount of experimental[3−11] and theoretical[12−28] work has been devoted to gaining an understanding of GFP photophysics. Nevertheless, a clear relationship between structure and photophysical properties has not been established yet, and a rationalization of the effects of chemical changes inside or around the chromophore is lacking. In particular, no understanding of the ECFP optical properties can be directly derived from the analysis of GFP photophysics. This is why we have undertaken the present project. In this study we address two limited questions as a first step in the interpretation of the photophysical properties of ECFP:

- describe the structures of the two different conformations known for ECFP (called A′ and B′; see below), particularly, the H-bond network around the chromophore within the following simplifying hypotheses: only the standard protonation states (for pH 7) of titratable residues are considered, the chromophore is assumed to be neutral, and there is no proton transfer involving the chromophore.

- determine the absorption spectrum of the chromophore embedded in the protein, compare the spectra obtained in the two conformations of the protein, identify the factors that might bring a difference between these two spectra, and provide an interpretation of the experimental double hump. In this first step we will not attempt to determine the vibrational structure of the spectrum.

First, we performed a 1 ns molecular dynamics (MD) simulation of the protein in an aqueous solvent to analyze the dynamics of the chromophore in the protein environment and the hydrogen-bond network in its surroundings. Then we determined the electronic absorption spectrum using quantum mechanical calculations of the vertical excitation energy of the chromophore in the electric field of the hydrated protein. These quantum mechanical calculations were performed on a series of 160 snapshots extracted along the MD trajectories.

Such a combination of classical dynamics and quantum mechanics does not consist of a truly consistent QM/MM treatment involving appropriate feedback from the QM to the MM parts.[29−31] The type of calculation performed here has already been used in the literature.[32,33] The present work is the first theoretical one on an ECFP chromophore embedded in a realistic environment.

ECFP presents a 3D structure very similar to that of GFP. All of these proteins consist of a 11-stranded β barrel, which is a nearly perfect cylinder (4.2 nm long and 2.4 nm in diameter, Figure 1).

* Corresponding author. E-mail: jacqueline.ridard@lcp.u-psud.fr.

10.1021/jp054656w CCC: $30.25
Published on Web 11/25/2005

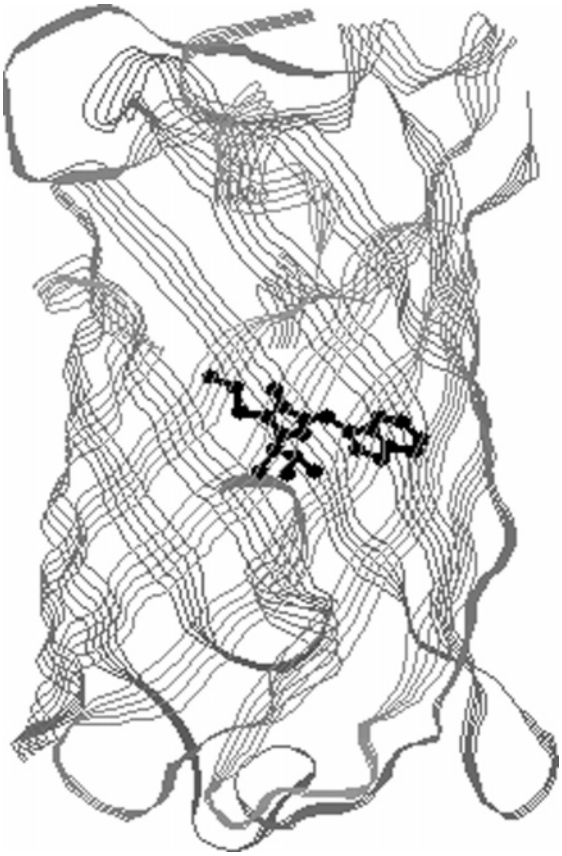

Figure 1. Schematic view of the enhanced cyan fluorescent protein. The chromophore is shown in atomic detail.

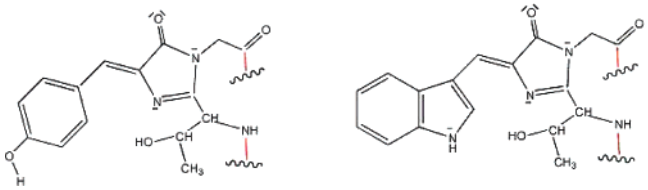

Figure 2. Chromophore structures of S65T GFP (left) and ECFP (right).

The chromophore is formed by cyclization−dehydration−oxidation of three amino acids at positions 65-66-67; see Figure 2. It is buried inside the barrel, carried by a central helix. In wild-type GFP, the three amino acids implied in the formation of the chromophore are Ser-Tyr-Gly. The mutations in ECFP with respect to wild-type GFP are (i) the replacement of Tyr66 by Trp66, resulting in changing the phenol ring of the chromophore into indole, (ii) the replacement of Ser65 by Thr65, affecting the nonconjugated part of the chromophore, and (iii) a series of mutations outside the chromophore[1]—F64L, N146I, M153T, and V163A.

The ^{19}F NMR study of ECFP reveals a slow exchange between two conformations with a characteristic time on the order of 1 ms.[34] The authors suggest the existence of either two different conformations of the chromophore itself or, and more probably, the existence of two conformations of a neighboring residue, His148, whose lateral chain could be oriented either toward the chromophore or toward the solvent.

The high-resolution X-ray structure of ECFP has been determined.[35] It shows two distinct conformations: a major one A′ and a minor one B′ with different orientations of the lateral chains of at least four residues, including His148 as suggested in Seifert et al.[34] The orientation of the lateral chains of these residues (the residues at positions 145-148 in strand 7 according to the numbering of Helms et al.[12]) is described in Table 1; the different orientations that are found indicate a high flexibility in that region.

TABLE 1: Orientation of the Lateral Chains of Four Residues of ECFP, Differing between forms A′ and B′

residue	orientation with respect to barrel[a]	
	A′	B′
Tyr145	in	parallel
Ile46	out	in
Ser147	in	out
His148	out	parallel

[a] In means that the lateral chain is oriented inside the barrel, out means that the lateral chain is oriented outside the barrel (embedded in the solvent), and parallel means that the lateral chain lies roughly on the wall of the barrel.

Excitation and emission wavelengths are found at 436 and 476 nm with the particular feature of the double hump[34−36]. Precise analysis of emission decay shows that at least four emitting species coexist,[36] but no structural characterization of these optically distinct species has been done until now. The question arises as to whether the two maxima of the absorption spectrum are related to A′ and B′ conformations.

Recent experimental results concerning a variant of ECFP[37] bring some indirect information concerning this question. In fact, the main mutation of this variant with respect to ECFP is the replacement of His148 by an aspartic acid, which is expected to stabilize a single conformation because the hydrophilic lateral chain of Asp should always be solvent-exposed. The absorption spectrum of this variant is found to be similar to that of ECFP, exhibiting two humps at the same wavelengths. This result is an indirect indication that the double hump of ECFP should not be due to the existence of the two conformations A′ and B′. However, this is not a direct proof; in particular, the X-ray structure of this mutant is not yet established, and it cannot be excluded that it presents different conformations such as ECFP.

2. Molecular Dynamics Calculations

2.1. Force Field Parameters. The AMBER force field[38] (hereafter referred to as *ff99*) was used for all standard amino acids. However, a specific force field had to be developed for the chromophore.

We started with a geometry optimization of the chromophore in its electronic ground state by means of an ab initio DFT calculation (B3LYP/6-31G*)[39] using a chromophore model that preserves the two peptide bonds between the chromophore and the neighboring residues (Leu64 and Val68), the α-carbons of these residues being replaced by hydrogen atoms (Figure 3).

Concerning the indole ring and the two chains linking the conjugated part of the chromophore to the protein (which are parts of the threonine and glycine residues incorporated into the chromophore), it appears that the equilibrium geometry parameters obtained in this way are very similar to those of *ff99* for the indole ring of Trp, Thr, and Gly. Thus, we have taken the *ff99* parameters (except atomic charges) for these parts of the chromophore.

Concerning the imidazolinone ring and the bridging bonds, we have used the values of bond lengths and angles of the optimized geometry, and we have derived van der Waals parameters and force constants (for bonds, angles, and dihedral constants) from *ff99* except for the torsion around the two bridging bonds (angles φ and τ; Figure 3), which we have determined separately.

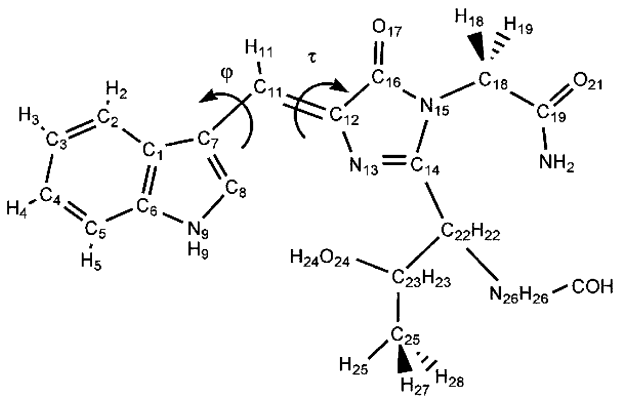

Figure 3. Chromophore model used for geometry optimization and force field parametrization.

The torsion is described in *ff99* by the expression

$$E_{\varphi} = k_{\varphi}[1 + \cos(2\varphi - \varphi_0)]$$

for the angle φ and by a similar expression for τ. The parameters k_{φ}, φ_0, k_{τ}, and τ_0 were adjusted by a least-squares fit on a set of DFT energies (for values of τ and φ varying in an interval of 20°). It results in the following values:

$$k_{\varphi} = 1.75 \text{ kcal/mol} \qquad k_{\tau} = 4.25 \text{ kcal/mol}$$

$$\varphi_0 = 180° \qquad \tau_0 = 180°$$

The value of k_{φ} is similar to the one determined by Reuter et al.[13] for the neutral chromophore of GFP (1.4 kcal/mol). The value of k_{τ}, which corresponds to the rotation around the bridging bond linked to the imidazolinone ring, is significantly smaller here than the one found for GFP (6.8 kcal/mol),[13] indicating a softer mode.

Atomic charges of the chromophore have been adjusted on the ab initio molecular potential calculated at the RHF/6-31G* level. The following constraints were imposed thanks to a specific program written by two of us (B.L. and J.R.):[40] (i) The sum of the charges of the NH2 and COH groups capping the chromophore is constrained to be zero so that the total charge of the chromophore residue, the entity used by the AMBER program (i.e. the chromophore model of Figure 3 minus these NH2 and COH groups), is zero. (ii) The charges of the atoms involved in the two peptide bonds (N26, H26, C19, O21) are constrained to be equal to those of the standard amino acid residues in *ff99*. The results are shown in Table 2.

The values of the charges of the indole ring are close to those of *ff99* for tryptophan; the amplitude of the differences ranges from 0 to 0.16 au (the latter in the case of C8), and the average is equal to 0.04 au. The charges of the lateral chain issued from threonine (from C23 to H24 in Table 2) are similar to those of *ff99* for threonine; the amplitude of the differences ranges from 0.004 to 0.071 au (the latter in the case of H24), and the average is equal to 0.03 au. With regard to the imidazolinone ring, our values can be compared with those adjusted on the RHF/6-31G* electrostatic potential of the chromophore of GFP;[14] the amplitude of the differences ranges from 0.02 to 0.13 au (the latter in the case of N13), and the average is equal to 0.07 au. However, they are significantly different (the average of the amplitude of the differences equals 0.3 au) from the ones adjusted for the interaction energy between the chromophore of GFP and water molecules.[13]

2.2. Simulation Details. Molecular dynamics was run using AMBER version 7.[41] Starting coordinates were taken from the Protein Data Bank: 1OXD entry for the major conformation A′ and 1OXE for the minor conformation B′. Missing heavy atoms and hydrogen atoms were added using the Leap program of AMBER. Aspartic and glutamic acids, lysine, and arginine residues have been taken in their standard states at neutral pH (charge −1 for Asp and Glu, charge +1 for Lys and Arg). All histidine and tyrosine residues have been taken in their neutral states. The protonation of the histidine imidazole ring was assigned in the same way as by Helms et al.[12] in their study of GFP. In fact, particular attention was given to His148, whose lateral chain does not have the same position in conformations A′ and B′. Inspection of the X-ray structures shows that the best protonation site for A′ is δ, whereas there is no valuable argument in favor of either site for B′, and we have arbitrarily

TABLE 2: Atomic Charges of the Chromophore of ECFP Used Here Compared to Other Values in the Literature[a]

	atomic charges (au)		
	present work	AMBER[41]	
	Link to LEU64		
N26	−0.41570	−0.4157	(peptide bond)
H26	0.27190	0.2719	
C22	−0.39707		
H22	0.21182		
C23	0.33077	0.3654	(THR residue)
H23	0.04817	0.0043	
C25	−0.25131	−0.2438	
H25	0.08657	0.0642	
H27	0.09964	0.0642	
H28	0.11244	0.0642	
O24	−0.64672	−0.6761	
H24	0.33885	0.4102	
	Link to VAL68		
C18	0.15253		
H18	0.05334		
H19	0.04641		
C19	0.59730	0.5973	(peptide bond)
O21	−0.56790	−0.5679	

		ref 13	ref 14
	Imidazolinone		
C14	0.32348	0.76	0.40
N13	−0.39296	−0.55	−0.52
C12	−0.05180	0.24	0.07
N15	−0.10576	−0.64	−0.03
C16	0.46447	−0.80	−0.53
O17	−0.59701	−0.61	−0.53

	present work	ref 41
	Bridging atoms	
C11	−0.06070	
H11	0.17268	
	Indole	
C7	−0.10304	−0.1415 (TRP residue)
C8	0.00202	−0.1638
H8	0.18919	0.2062
N9	−0.42908	−0.3418
H9	0.39728	0.3412
C6	0.24125	0.1380
C5	−0.32187	−0.2601
H5	0.17550	0.1572
C4	−0.11713	−0.1134
H4	0.15660	0.1417
C3	−0.20521	−0.1972
H3	0.16517	0.1447
C2	−0.23843	−0.2387
H2	0.17463	0.1700
C1	0.08968	0.1243

[a] Atom labels are given in Figure 3.

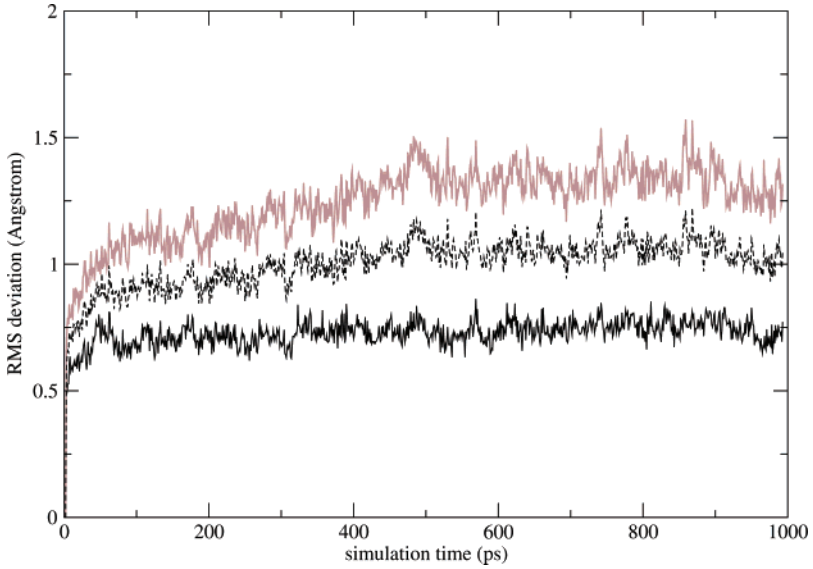

Figure 4. The rms deviations from the X-ray structure for conformation A′. Dark line: α-carbons of the central helix and the β-sheets. Red line: remaining α-carbons. Dashed line: all α-carbons of the protein.

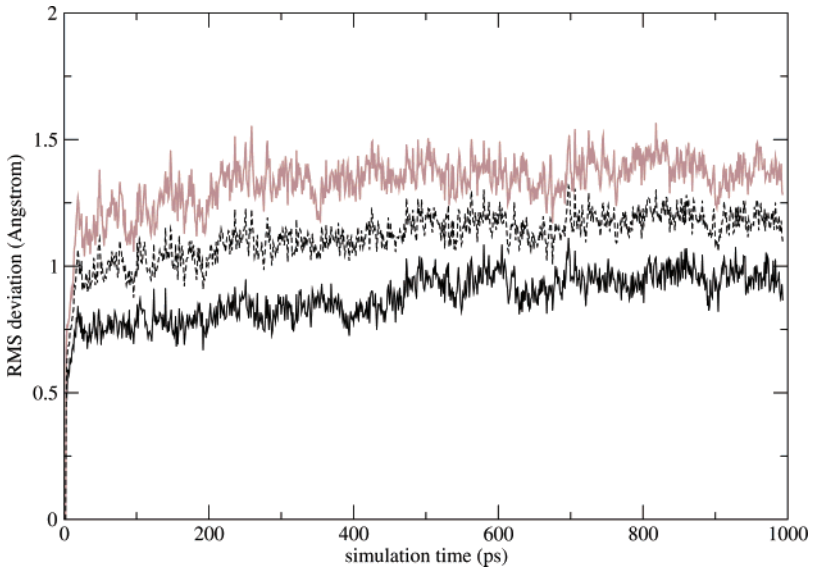

Figure 5. Same data as in Figure 4 but for conformation B′.

chosen the δ site. Six Na^+ ions were added to neutralize the protein; all of them are localized far from the chromophore and its neighbors so that they introduce no additional difference between A′ and B′. The system was solvated in a TIP3P water box with a distance of 8 Å between the walls of the box and the closest atoms of the protein. The total number of water molecules, including the 166 water molecules present in the crystallographic structures, is 8291 for the major conformation and 8418 for the minor conformation. The initial dimensions of the box are 60 × 76 × 77 $Å^3$ and 62 × 76 × 77 $Å^3$, respectively. The particle-mesh Ewald procedure[42] available in AMBER has been used to deal with long-range electrostatic interactions. (It might be argued that the Ewald procedure involves the improper assumptions of periodic boundaries;[43] this point was not examined here. However, a recent related study[44] concludes that there is no artifact due to periodic boundaries in the linear-scaling Ewald method.) The cutoff used for the calculation of the van der Waals interactions and for the direct sum of electrostatic interactions was set to its default value in AMBER (8 Å).

The energy of the whole system was initially minimized at constant volume: optimization of the positions of the hydrogen atoms was followed by optimization of the whole system. The whole system is then heated at constant volume from 100 to 300K using the Berendsen coupling algorithm (60 ps). Constant-pressure dynamics (1 atm) at 300 K follows until 1000 ps. A 1 fs time step was used all along the dynamics, and bonds involving hydrogen were constrained using the SHAKE algorithm.

2.3. Molecular Dynamics Results. *Comparison with X-ray Structures*. The structures obtained along the MD calculation have been compared with the X-ray structures by evaluating a series of rmsd's (root-mean-square deviations); see Figures 4 and 5.

The following main features appear in these two Figures:

(i) For the α-carbons of the residues belonging to the β sheets and to the central helix carrying the chromophore (dark lines), it appears that the rmsd rapidly reaches a stable value close to 0.75 Å (standard deviation of rmsd from the average value: 0.04 Å) for the major conformation A′. Concerning conformation

TABLE 3: Variations of the Two Rotation Angles Defined in Figure 3[a]

	A′	B′	vacuum
$\langle\varphi\rangle$	−6°	−4.7°	−0.2°
$\sigma(\varphi)$	7.9°	8.8°	11.3°
$\langle\tau\rangle$	−1.7°	−1.9°	0.2°
$\sigma(\tau)$	7.4°	7.3°	8.2°

[a] Columns A′ and B′ present the results of the MD simulation for the two conformations (A′ and B′) of ECFP, and the column labeled vacuum presents the results obtained after an MD calculation of the chromophore alone in vacuum using the same conditions (time step, time length, temperature, potential, ...) as the ones used for either of the conformations of ECFP.

B′, this deviation first reaches a value of about 0.80 Å (standard deviation: 0.05 Å) in the time interval 100−500 ps and then increases to 0.95 Å. It has not been possible to identify the nature of the motion occurring around 500 ps after the start of the simulation. Nevertheless, the rmsd values obtained here indicate a stable structure of the β sheets, as expected.

(ii) The deviations of the α-carbons of the remaining residues (helices and flexible loops at the tops of the barrel; red lines) have a much larger amplitude, reflecting the flexible character of these parts of the protein.

(iii) The rmsd's for all α-carbons simultaneously (dashed lines) remain in the interval 0.90−1.20 Å during the simulation for both conformations. These values are larger than the ones found in i because of the contribution of the atoms described in ii; they have the same order of magnitude as the ones obtained for GFP but are slightly larger (0.9 Å in Helms et al.,[12] 0.75−0.91 Å in Reuter et al.,[13] and 0.70−0.75 Å in Nifosi et al.[14]).

We conclude that the simulation protocol used here results in the usual values of rms deviations and that the present simulation is consistent with the X-ray structures.

All along the simulation, the orientations of the lateral chains of the four residues (145−148) remain consistent with the X-ray structures; an exchange between conformations A′ and B′ is not observed during the 1 ns simulation, which is consistent with the NMR study[34] indicating a time scale of about 1 ms for the conformational exchange.

In conclusion, the structures of conformations A′ and B′ of ECFP resulting from the present simulations are consistent with X-ray structures.

Internal Dynamics of the Chromophore: Description. An important outcome of the present simulation concerns the dynamics of the chromophore in protein as compared to the dynamics in vacuum. In fact, it appears that the internal rotations around the bridging bonds, described by the angles φ and τ (Figure 3), are partially quenched by the protein. This can be seen by comparing the values of the average and standard deviations of these angles when the chromophore is embedded in ECFP with the corresponding values obtained with the chromophore alone in vacuum (Table 3 and Figure 6).

The quenching is particularly clear for the angle φ: values of φ larger than about 10° appear to be forbidden in proteins, whereas they are actually reached in vacuum. Nothing similar occurs for the negative values of φ. As a result, the standard deviation of φ in proteins is divided by a factor of between 1.4 and 1.3 with respect to the value in vacuum, and the average value is shifted by an amount smaller than the standard deviation in vacuum. The corresponding variations for τ are much smaller, but it can be seen that the ratio of the shifts of φ and τ is roughly proportional to the inverse ratio of the force constants: one has $k_\tau/k_\varphi = 2.4$, whereas the ratio between shifts $\delta\langle\varphi\rangle$ and $\delta\langle\tau\rangle$ between vacuum and ECFP is $\delta\langle\varphi\rangle/\delta\langle\tau\rangle = 3.0$ in conformation A′ and 2.1 in conformation B′. This is similar to what is obtained with two sequential springs holding a weight. It indicates that, mainly, a single effect is at the origin of the internal rotation of the chromophore in protein with respect to planarity and that the different responses of the angles φ and τ simply reflect the different hardness of the potential with respect to rotation around these two angles. That effect is probably also at the origin of the decrease of the standard deviations, that is, the amplitude of the internal motions of the chromophore in protein with respect to the amplitude in vacuum. It can be expressed roughly that ECFP forces in some way cause the chromophore to twist slightly and hold it in the twisted position.

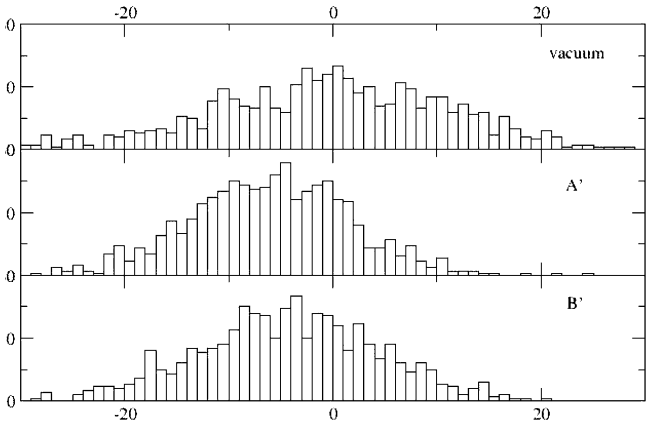

Figure 6. Distribution of angle φ during MD simulation of the chromophore alone (top) or embedded in the protein: conformation A′ (middle) or B′ (bottom).

In addition, we note that, for both conformations, the imidazolinone and indole rings remain nearly planar during the simulation; all dihedral angles have average values in the interval (−2°, +2°), with standard deviations in the range (5°, 7°) similar to that in vacuum. Thus, the action of the protein can be described as a torque exerted on the two rigid rings.

Internal Dynamics of the Chromophore: Discussion. More insight into the dynamics of the chromophore can be obtained by evaluating separately the interaction between the chromophore and each residue of the protein. This interaction can be characterized by the torque defined as $-\partial E_{res}/\partial\varphi$, where E_{res} is the interaction energy between the chromophore and residues (res) and φ is the twist angle defined in Figure 3. (The angle φ is more significant than τ as just seen, and we consider only φ here.) The torque has been evaluated for the snapshots extracted every 5 ps (160 snapshots) and, each time, for the two extreme values that can be reached by φ at a given temperature in the situation where all of the remaining degrees of freedom of the system are frozen.

More precisely, we evaluated the energy difference $E - E_{MD}$, where E_{MD} and E are the energies of the whole system (chromophore, protein, water, counterions,...) corresponding, respectively, to $\varphi = \varphi_{MD}$ (the value of φ in the considered snapshot) and to varying values of φ. Then, we determined the two values of φ such that the Boltzmann factor $B = \exp[-(E - E_{MD})/kT]$ is sufficiently small. (In practice we have used $B \approx 10^{-2}$ and $T = 300$ K, the temperature used in the MD simulation.) There are two such values, one with $\varphi - \varphi_{MD} = \delta\varphi > 0$ and the second with $\delta\varphi < 0$. Depending on the snapshot, one finds $|\delta\varphi| \approx 6-7°$, a range consistent with the results shown in Table 3 and Figure 6.

Table 4 presents the two lists of residues (one for conformation A′ and one for conformation B′) that give rise to the largest average values of the torques over the 160 snapshots. It is first

TABLE 4: List of Residues Applying the Largest Torques on the Chromophore and Average Values of the Torques (kcal/mol/deg) over 160 Snapshots[a]

conformation A′				conformation B′			
$\delta\varphi > 0$		$\delta\varphi > 0$		$\delta\varphi > 0$		$\delta\varphi > 0$	
Ile167	0.56	Val150	−0.62	Ile167	0.49	Val150	−0.61
Phe165	0.25	Glu222	−0.24	Phe165	0.18	Thr203	−0.28
Glu222	−0.18	Thr203	−0.18	W117	0.12	Glu222	−0.22
Thr62	0.11	Asn149	−0.10	His148	0.09	W117	0.05
W118	0.10	W118	−0.05	Thr64	0.07		
Tyr145	0.06	His148	−0.05	Thr203	0.05		
Thr203	0.06						
Asn149	0.05						

[a]For each snapshot, the torque is evaluated at the extremum values $\varphi_{MD} + \delta\varphi$ of the twist angle φ in either direction with respect to the value φ_{MD} in that snapshot. The extremum values are defined by the condition that the Boltzmann factor $B = \exp[-(E - E_{MD})/kT]$ at $T = 300$ K is equal to 10^{-2}.

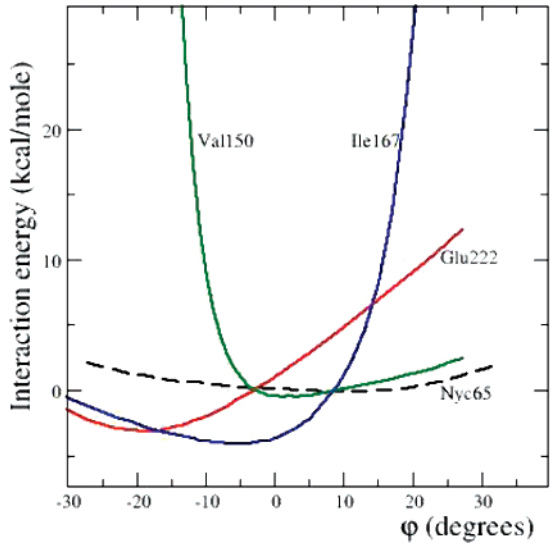

Figure 7. Interaction energy between the chromophore (Nyc65) and different residues for varying values of the twist angle φ in a given snapshot of conformation A′. The broken line refers to the twist energy of the chromophore alone (energy difference between the current value of φ and the value of φ in the snapshot, namely, $\varphi = 2.8°$).

seen that only a limited number of residues contribute significantly, that is, more than the chromophore alone. (The magnitude of the torque of the chromophore alone is in the range 0.05−0.1 kcal/mol/deg, depending on the snapshot.) These residues are mainly Ile167 and Val150 and, to a smaller extent, Phe165, Thr203, and Glu222. The different types of interactions can be understood by considering the variation of interaction energy with φ (in a single snapshot and only for conformation A′) shown in Figure 7.

It is seen in Figure 7 that the interaction between the chromophore and Ile167 or Val150 is strongly repulsive on one side and weakly attractive on the other side; this is why these residues appear in the list in Table 4 in a single direction—the one where the interaction is strongly repulsive. In fact, these two residues are hydrophobic, and the repulsion comes from the short-range van der Waals interaction between their aliphatic chains and the chromophore. An interaction of the same type is found with Phe165 and Thr203 (although the interaction between the chromophore and Thr203 is partly electrostatic because of the hydroxyl group of Thr203). Similar short-range repulsions arise in conformation B′. In contrast, the interaction energy between the chromophore and Glu222 has a minimum value of $\varphi = -18.5°$ due to the fact that the oxygen atoms of

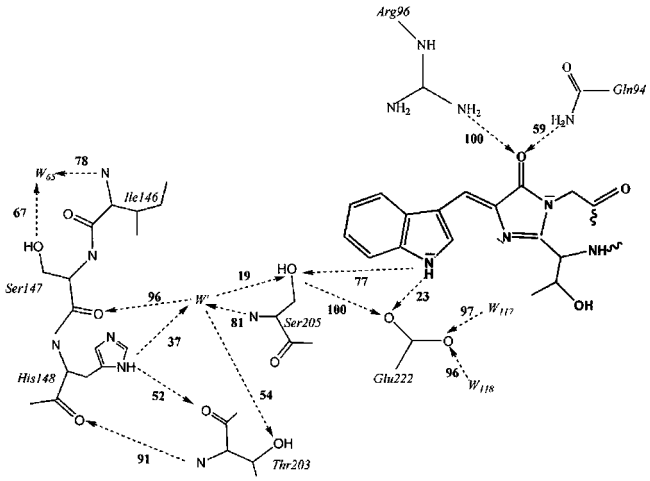

Figure 8. Part of the H-bond network in conformation A′. The numbers give the H-bond occupancies in percent during the 1 ns simulation (cutoff: 3.2 Å for distances, 40° for angles). Arrows point from H-donor to H-acceptor atoms.

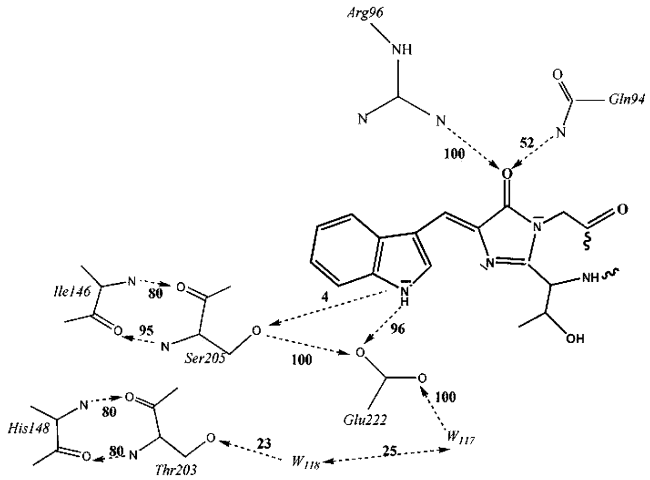

Figure 9. Same as Figure 8 for conformation B′.

the carboxylic group CO_2^- of Glu222 and the H9 atom of the chromophore have an attractive electrostatic interaction and the CO_2^- group does not lie exactly in the chromophore plane; this situation explains why the torque is always negative when φ ranges from −7 to 7° in conformation A′. (The situation for Glu222 is different in conformation B′, where one of the oxygen atoms of the CO_2^- group lies in the chromophore plane and therefore does not contribute to the torque.) The remaining residues give negligible torque values similar to the results in Table 4. In particular, the residues giving rise to a permanent H bond with the chromophore (Figures 8 and 9) do not contribute to the torque because these H bonds lie in the chromophore plane and give rise to a torque only if $|\varphi|$ is large enough, a situation that is not explored because of the repulsion by Ile167 and Val150.

Finally, it appears that the twist of the chromophore is not controlled by its own twist potential, by the permanent H bonds, or by the electrostatic attractions such as the one coming here from Glu222. In fact, the driving force for this twist comes from the strong short-range repulsion by the four residues (Ile167, Val150, Phe165, and Thr203) surrounding the average position of the chromophore; the motion of these four residues determines the small allowed domain of the twist angle φ through their strong repulsive interactions with the chromophore at short distances.

We conclude that ECFP modifies the dynamics of the chromophore for that which concerns torsion around the bridge. However, the magnitude of this effect is small and might not be sufficient to disturb the electronic structure strongly in either the ground or the excited state (section 3 below).

Hydrogen Bond Network near the Chromophore. A schematic view of the H-bond network resulting from our simulation is presented in Figure 8 for conformation A′ and in Figure 9 for conformation B′. These two Figures concern mainly the region near the chromophore, where ECFP presents significant differences with GFP and also conformation A′ with conformation B′.

It is first seen that the H bond involving nitrogen N9 of the indole ring differs between the two conformations: in A′, N9 is strongly bonded to the hydroxyl oxygen of Ser205 (77% of the time) and weakly bonded to one of the carboxylic oxygens of Glu222 (23% of the time), whereas the inverse situation is observed in B′. (N9 is bonded 4% of the time with Ser205 and 96% of the time with Glu222.)

This difference is clearly related to the different H bonds of Ser205. In fact, the simulation of B′ shows that both Ser205 and Thr203 (strand 6) are linked by the two backbone H bonds expected in a perfect β-sheet structure with the adjacent residues of strand 7 (Ile146 and His148, respectively). However, no H bonds exist between Ser205 and Ile146 in A′, and it also appears that the orientation of the lateral chain of His148 in this conformation cannot coexist with standard backbone H bonds: there are two H bonds between Thr203 and His148, but one of them involves an N atom of the lateral chain of His148 (52% of the time) instead of the backbone N atom. In fact, it is well known that the β-sheet structure of the barrel is partly broken between strands 6 and 7 in all GFPs. It appears here that in ECFP the β structure is preserved in the surroundings of the chromophore in conformation B′ and is almost completely broken in conformation A′.

The specific positions of the lateral chain of His148 and the cleft between strands 6 and 7 in conformation A′ are also related to the position of the water molecule coined W′ in Figure 8. This molecule is not one of the crystallographic water molecules found in the X-ray structure. It lies just outside the wall of the barrel at the beginning of the simulation and then moves to the cleft between strands 6 and 7 after about 150 ps and remains in that position, never really going inside the barrel. Thus, it might have moved only after an appropriate fluctuation of His148, which is not tightly bound to the residue of the adjacent strand. Nothing similar occurs in conformation B′, where His148 is tightly bound as in GFP.

Another difference between conformations A′ and B′ concerns the five crystallographic water molecules closest to the chromophore (W55, W117, W118, W162, and W163). They form a H-bond network among each other and with neighboring residues; this network is more rigid in conformation A′ than in conformation B′. For instance, in A′, W163 is involved in three H bonds (with W118, Gln69, and W162) more than 85% of the time, whereas in conformation B′, none of the H bonds where it is involved exists more than 55% of the time.

The simulation also provides some insight into the bonds ending at the hydroxyl group of Thr65 (O24−H24; Figure 3). This OH group is H bonded with the carboxylic group of Glu222 in all of the variants of GFP[12−14]. However, Nifosi and Tozzini[14] have found, for the neutral chromophore of GFP, a rather unstable configuration of this hydroxyl group with a H bond flipping between Glu222 and the backbone oxygen atoms of Val61 or Leu64 (5% of the time on the latter two). They ascribe this unstable configuration to the large number of van der Waals interactions possible for the methyl group of Thr65. In contrast to this situation, we have found no strong H bond involving this hydroxyl group and only weak bonds with the backbone oxygen atoms of Val61 and Leu64, probably reflecting the different positions of Glu222 in GFP and ECFP.

3. Quantum Mechanical Calculations

The second goal of this work concerns the interpretation of the absorption spectra of ECFP. In particular, it addresses the question of whether the double hump of the experimental spectrum is due to the two conformations A′ and B′ of that protein. To get information on this question, we have extracted a set of snapshots from the MD trajectories of each conformation. For each snapshot, we have determined the vertical transition energy and oscillator strength of the lowest electronic transitions of a chromophore model, defined as a truncated part of a protein using the TDDFT method.

A similar procedure has been used already.[32,33] The accuracy that can be expected is limited by several factors, mainly, the various choices and approximations made in the MD calculation (choice of the protonation states, choice of the force field, Ewald sum, and frozen charges. It has been seen in the previous section that our MD results are consistent with X-ray structures and that the simulated hydrogen-bond network does not exhibit any unexpected features), the (necessarily) limited number of snapshots, the approximations made in the QM calculations (TDDFT approach, specific choice of the density functional), and finally, the truncation of the chromophore. The latter amounts to neglecting several electronic effects including

- the effect of the polarization of the environment (the polarization varies upon electronic excitation of the chromophore because electronic excitation usually changes the charge repartition within the chromophore);

- and the effect of the dispersion interactions between the chromophore and the remaining protein, which varies also upon the electronic excitation of the chromophore. (Electronic excitation usually increases the polarizability significantly and therefore the dispersion interactions.)

The effect of environment polarization on the electronic transition energies has already been studied in the literature and has been found to be non-negligible. In the case of the absorption spectra of several polyene aldehydes in polar solvents,[45] this effect is found to be in the range 0.12−0.18 eV, and in the case of retinal in bacteriorhodopsin,[30] it has been evaluated at 0.18 eV. The uncertainty related to the TDDFT method can be as large as 0.5−1.0 eV (Wanko et al.,[46] Table 1).

But the energy separation corresponding to the two humps of the experimental absorption spectrum (at 437 and 451 nm[36]) is as small as 0.088 eV. Therefore, it is hopeless to find an interpretation of these humps on the basis of a purely quantitative comparison between theory and experiment because the latter appears to be much smaller because of a number of uncertainty factors. Although a quantitative comparison is useful, one has to clearly consider qualitative arguments also.

Therefore, we have used the TDDFT approach, even though it might be less accurate than alternative methods. In particular, in the case of charge transfer or a highly excited state, it is by far the fastest approach and seems to be a viable option,[25,47] especially for species that are too large to be studied easily by more accurate ab initio methods and/or preliminary studies. Concerning the density functional, we have used B3LYP, which is at present the most widely used one, and have compared it with BP86.

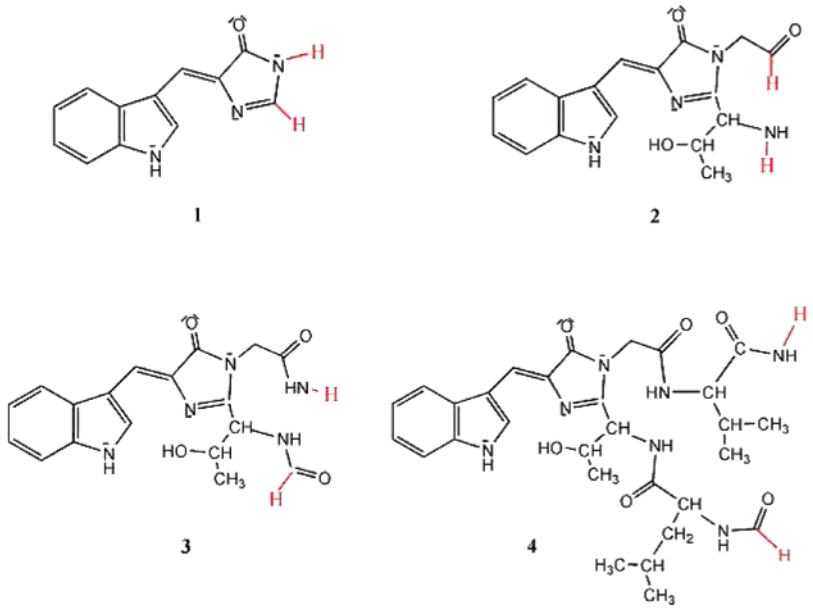

Figure 10. Four different models of the chromophore that have been tested.

TABLE 5: Wavelength of the Lowest Vertical Transition Obtained by TDDFT/B3LYP/6-31G* Calculations for the Different Chromophore Models Presented in Figure 10 in Vacuum

model	wavelength of the lowest-vertical electronic transition, nm
1	361
2	372
3	379
4	378

We have also checked the chromophore model and the effect of the truncation of the snapshot list. It is useful to note that additional sources of errors analyzed by Wanko et al.[46] have been explicitely taken into account here, for instance, the need for geometry optimization (which is replaced here by an average over the geometries visited along the MD trajectories) or the electrostatic effect of the environment.

Chromophore Model for Transition Energy Calculations. To study the electronic excitation properties of the chromophore, we first have to determine its appropriate extension; that is, we have to determine which covalent bonds between the chromophore and protein backbone must be cut. To that end, four models, presented in Figure 10, have been tested.

The geometry of each model was partially optimized, the links to the protein backbone always being frozen to remain in the geometry of the X-ray structure. Then, we evaluated the first active transition energy by TDDFT/B3LYP/6-31G*[39] calculations in vacuum. Results are given in Table 5.

The value obtained with model 4, which is the most extended one, can be considered to be the reference. Thus, it appears clearly that model 3 achieves the best compromise between size and accuracy, and it was retained.

In this model, the entire structure resulting from the Thr-Trp-Gly cyclization and the two amide bonds linking the chromophore to the protein are included, and the cuts take place at the single bonds between the amide groups and the α-carbons of the adjacent residues (Leu64 and Val68) with these α-carbons being replaced by hydrogen atoms. This model is the same as the one used in this work to determine force field parameters.

Calculation Details. Snapshots were extracted from the MD trajectories of the two conformations A′ and B′ every 5 ps, starting 200 ps after the beginning of the simulation and ending at 1 ns (160 snapshots). For each snapshot, vertical transition energies and oscillator strengths of the four lowest excited states of the chromophore model (covering the wavelength range of the experimental spectrum, 350−500 nm) were calculated using the same method as the one used for testing the chromophore model in vacuum (TDDFT/B3LYP/6-31G*). The calculations were carried out either in vacuum (calculation I) or in the presence of point charges representing the electrostatic effects of the environment of the chromophore in a protein (calculation II). These point charges are located on each atom of the system with a charge equal to that of the AMBER force field (*ff99*), and the charge set includes all of the atoms of the protein (with the exception of the atoms included in the chromophore model 3) as well as the crystallographic water molecules, solvent water molecules, and counterions inside the simulation box. Calculation II was also performed using the BP86 functional. In addition (calculation III), we have calculated the transition energies of the chromophore model in vacuum using snapshots extracted from MD trajectories in vacuum instead of MD trajectories in the presence of protein and water molecules as done in calculations I and II. The results are analyzed in the next two sections.

Electronic Transitions: Orbital Analysis. An orbital analysis of calculation II was performed to describe the nature of the active transitions. The most significant orbitals are shown in Figure 11.

An analysis of the main components of the electronic transitions resulting from the TDDFT/B3LYP/6-31G* calculations shows that two types of transitions may be active in both conformations of ECFP. First, the HOMO−LUMO transition appears in all of the considered geometries. It is seen in Figure 11 that the HOMO and LUMO orbitals are essentially of the π type and present strong similitudes with the corresponding orbitals of the neutral chromophore of GFP.[18,25] Both are essentially delocalized on the two rings (indole and imidazolinone) although to a different extent; they differ mainly by the bonding/antibonding pattern in the bridging region near atoms C11−C12 (Figure 3), which means that the π-bonding character of the C11−C12 bond is weakened upon excitation, implying that it becomes less rigid with respect to rotation. The wavelength corresponding to this transition extends from 370−

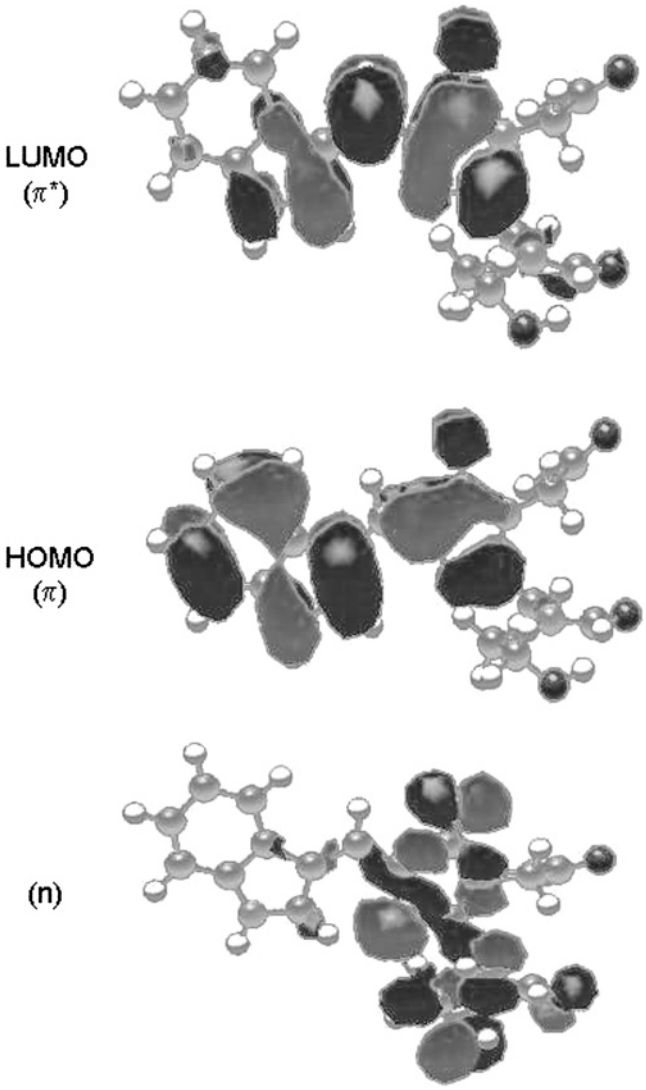

Figure 11. Different orbitals involved in the electronic transitions.

450 nm depending on the geometry and represents the main contribution to the absorption spectrum.

A second type of transition implies excitation from the σ n-type orbital of Figure 11 to the LUMO π^* orbital. This σ n-type orbital exhibits a strong character of lone pairs on oxygen O17 and nitrogen N13, located on the imidazolinone ring (Figure 3). These $n-\pi^*$ transitions have weak oscillator strengths. In some geometries, a mixing between both types ($\pi-\pi^*$ and $n-\pi^*$) occurs, resulting in two active absorptions (oscillator strength > 0.1).

Electronic Transitions: Absorption Spectrum. For both conformations A′ and B′, a histogram of the absorption wavelengths resulting from the TDDFT calculations (calculations I and II) was constructed, each contribution being weighted by the oscillator strength. The same histogram was also constructed for the chromophore in vacuum (calculation III). This type of histogram can be considered a low-resolution absorption spectrum (i.e., without vibrational structure). Determining a true high-resolution spectrum (i.e., with a resolution comparable with the experimental one) would require the determination of the Franck−Condon factors using the vibrational wave functions in both the ground and excited states and thus the study of the dynamics of protein by some type of quantum approach instead of the classical trajectories used here; this is beyond the scope of the present study. Thus, we have to compare a low-resolution theoretical spectrum with a higher-resolution experimental one. The results are shown in Table 6 and in Figure 12.

TABLE 6: Characteristics of Calculated Absorption Spectra Using Either the B3LYP or BP86 Density Functional Compared to Experimental Data[a]

	maximum	width
experimental	437 nm 451 nm	60 nm
B3LYP calculations		
calc I (A′)	390 nm	28 nm
calc I (B′)	390 nm	20 mn
calc II (A′)	400 nm	35 mn
calc II (B′)	400 nm	28 nm
calc III	380 nm	30 nm
BP86 calculations		
calc II (A′)	450 nm	41 nm
calc II (B′)	445 nm	41 nm
calc III	420 nm	39 nm

[a]Calculation I: dynamics of protein taken into account but electrostatic effects neglected; calculation II: both dynamics and electrostatic effects of protein taken into account; calculation III: dynamics of the chromophore in vacuum.

For both conformations A′ and B′, the TDDFT/B3LYP calculated spectrum (calculation II, taking into account the dynamic and electrostatic effects of the protein) exhibits a single peak located at 400 nm and a mid-height width about 30 nm (35 nm for A′ and 28 nm for B′). Thus, there is a blue shift of 37 and 51 nm (corresponding energy difference: 0.26 or 0.35 eV) between the theoretical location of the maximum and the two experimental humps.

With the TDDFT/BP86 functional, the spectra of A′ and B′ still remain indistinct; the maximum is now located at 450 nm, and the width is equal to about 40 nm. These results are in better agreement with experimental values than those obtained using the B3LYP functional. However, we have no theoretical argument in favor of the BP86 functional, and in view of the analysis by Wanko et al.,[46] an agreement better than 0.3 eV between TDDFT calculations and experiment can only be fortuitous. Therefore, the most likely interpretation of the different accuracies found here with different density functionals is that there is a nearly exact compensation between the different errors (inherent inacurracy of the functional and the different neglected effects mentioned at the beginning of section 3) with BP86 and an imperfect compensation with B3LYP.

Thus, the most significant result obtained here is that there is no difference between the positions of the absorption spectra of the two conformations A′ and B′ with either density functional.

Analysis. We present here some qualitative arguments supporting the main result of the previous section: there is no difference between the absorption spectra of A′ and B′.

Dynamic Effect of the Protein. We first examined the evolution of the spectrum from the chromophore in vacuum (calculation III) and compared it to that of the chromophore in the protein (calculation I) (cf. Table 6 and Figure 13). The difference between the spectra obtained in calculations III and I reflects the dynamic effect of protein on the chromophore, whereas the difference between the two spectra obtained in calculation I reflects the difference between the dynamic effects in conformations A′ and B′ of the protein. It is seen in Figure 13 that the three spectra of calculations I and III cover the same wavelength range (350−410 nm). The spectrum of the chromophore in vacuum (calculation III) is more intense in the region

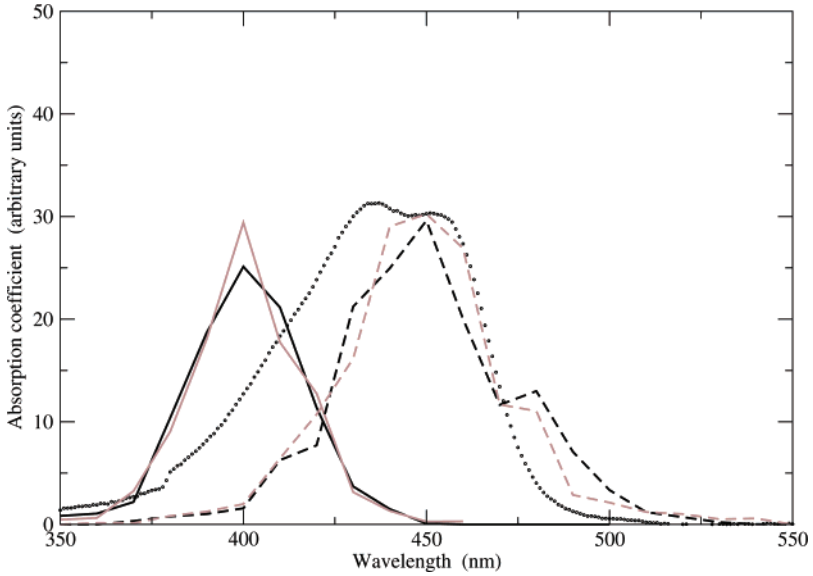

Figure 12. Comparison between the experimental absorption spectrum obtained at pH 7.4 and 20 °C (dotted line) and the theoretical spectra (calculation II) of conformation A′ obtained by using either the B3LYP (dark line) or the BP86 (dashed dark line) density functional and conformation B′ (red line for B3LYP, dashed red line for BP86).

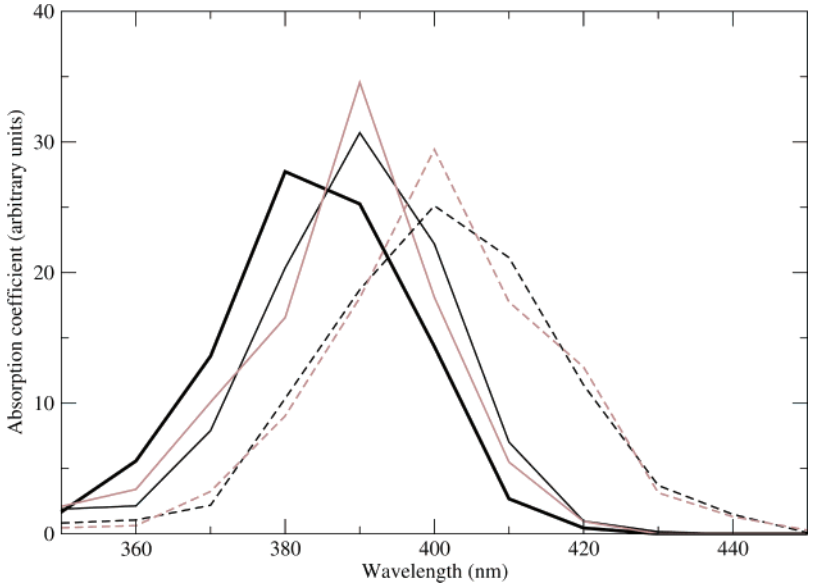

Figure 13. Comparison between the spectra obtained by TDDFT/B3LYP using snapshots extracted from MD simulations of the chromophore and the protein. Calculation I: dark line for A′, red line for B′. Calculation II: dashed dark line for A′, dashed red line for B′. Calculation III (MD simulation of chromophore alone in vacuum): thick dark line.

of low wavelengths, whereas the two spectra taking into account the dynamic effect of the protein are more intense in the region of large wavelengths, resulting in a red shift of the absorption maximum of about 10 nm.

Electrostatic Effect of the Protein. The effect of the electrostatic interactions between the chromophore and the environment (difference between calculations I and II) results in an additional red shift of 10 nm for both spectra so that the maxima of the two conformations still remain indistinct. This small shift reflects the fact that the electronic transitions involve a very limited charge transfer.

In fact, it can be explained by evaluating the energy of the partial charges for both the ground and the excited states of the chromophore (the charges for the excited state were determined by using the same method as the one used for the ground state; see section 2.1 and a CIS wave function[39]) in the potential created by the charges of the atoms of the protein. Thus, the electrostatic effect on the difference between the two spectra appears as a sum over the atoms of the chromophore: $\delta = \sum_{at}[V_{at}(A') - V_{at}(B')][q_{at}(S_0) - q_{at}(S_1)]$ with self-explanatory notations.

In fact, the main difference in the vicinity of the chromophore between the two forms A′ and B′ of the protein is the replacement of Ser205 by Glu222 as the partner in the H bond with N9, which means that the largest factor $V_{at}(A') - V_{at}(B')$ is obtained for N9 or H9. Thus, one could have expected that N9 would yield a large contribution to the difference between the electrostatic effect, but this does not hold because the charge of N9 is nearly the same in the ground state and the excited state as can be expected from Figure 11. In addition, the atoms with a significant charge difference between the two electronic states, namely, the bridging carbon atom C11 (Figure 3) and the carbon atoms of the six-membered ring of indole, are a large distance away from Ser205 and Glu222, and they yield a small difference between the electrostatic effect in the two conformations.

These two circumstances provide a qualitative explanation of the fact that the electrostatic effect shifts the spectra of the two conformations by approximately the same amount.

The electrostatic effect also yields a significant broadening of the spectra of about 8 nm; it reflects the fluctuations of the proteic environment.

Neglected Effects. We will now evaluate the order of magnitude of the effect $\delta\Delta E$ of the polarization of the protein (induction effect) and the dispersion interaction between the protein and the chromophore on the transition energy. These two effects are additive, and one has $\delta\Delta E = \delta_{ind}\Delta E + \delta_{disp}\Delta E$; in addition, each of the induction and dispersion effects may be written in the form of a sum of contributions, one for each residue. Let $\gamma_{ind}(R)$ be the contribution of residue R to induction and $\gamma_{disp}(R)$ the contribution of that residue to dispersion:

$$\delta\Delta E = \delta_{ind}\Delta E + \delta_{disp}\Delta E = \sum_R \gamma_{ind}(R) + \gamma_{disp}(R)$$

One gets (retaining only the dipolar contributions) (cf. A. J. Stone[48])

$$\gamma_{ind}(R) = -\frac{\mu_1^2[1+3\cos(\theta_{1,R})^2] - \mu_0^2[1+3\cos(\theta_{0,R})^2]}{2}\frac{1}{(4\pi\epsilon_0)^2}\frac{\alpha_R}{\rho_R^6} \quad (1)$$

$$\gamma_{disp}(R) = -\frac{3}{2}\left(\frac{U_1\alpha_1}{U_1+U_R} - \frac{U_0\alpha_0}{U_0+U_R}\right)\frac{1}{(4\pi\epsilon_0)^2}\frac{U_R\alpha_R}{\rho_R^6}$$

where μ_0 and μ_1 are the dipole moments of the chromophore in its ground and excited states, respectively; α_0, α_1, and α_R are the dipole polarizabilities (assumed to be isotropic) of the chromophore in the two states and of the residue R; U_0, U_1, and U_R are the average electronic transition energies; $\theta_{0,R}$ and $\theta_{1,R}$ are the angles between the dipole moments of the chromophore in the two states and the axis joining the chromophore to the residue R; ρ_R is the distance between the chromophore and the residue R; and ϵ_0 is the vacuum permittivity.

The quantum mechanical calculation easily yields values for the dipole moments μ_1 and μ_0. Here, it was found (DFT calculation for the ground state and CIS for the excited state) that these two moments are nearly parallel (angle smaller than 1°); accordingly, one gets

$$\gamma_{ind}(R) = -\frac{\Delta\mu^2\,[1+3\cos(\theta_{0,R})^2]}{2}\frac{1}{(4\pi\epsilon_0)^2}\frac{\alpha_R}{\rho_R^6} \qquad \Delta\mu^2 = \mu_1^2 - \mu_0^2$$

One might then get the order of magnitude of $\delta_{ind}\Delta E$ by assuming that the protein is a homogeneous medium with a uniform density of residues and polarizabilities (continuum model). It allows the replacement of the sum over residues by a volume integration giving

$$\delta_{ind}\Delta E = -\frac{\Delta\mu^2\bar{\alpha}}{2(4\pi\epsilon_0)^2}8\pi\frac{1}{3\rho_{min}^3}$$

where $\bar{\alpha}$ is the density of polarizability and ρ_{min} is a cutoff in the radial integration accounting for the fact that there is a nonvanishing minimum distance between the chromophore and any residue.

However, one is more interested here in determining whether induction contributes to the separation of the transition energies of the two conformations, A′ and B′, of ECFP rather than to the prediction of accurate values of these energies (which are known experimentally within an uncertainty on the order of 0.09 eV corresponding to the separation of the two experimental humps). From the above structure analysis (section 2.3), the main difference between these two conformations comes from the nature and position of the residues lying in the direction from N9 to Ser205 and Glu222. Thus, it is convenient to use the two following additional hypotheses (within the continuum model):

- The average density of polarizability $\bar{\alpha}$ is the same in both conformations except inside the solid angle Ω delimited by N9, Ser205, and Glu222.

- Inside Ω, the densities of polarizability $\bar{\alpha}_A$ and $\bar{\alpha}_B$ of the two conformations are slightly different; they satisfy

$$\frac{\bar{\alpha}_A + \bar{\alpha}_B}{2} = \bar{\alpha} \qquad \Delta\bar{\alpha} = |\bar{\alpha}_A - \bar{\alpha}_B| < \bar{\alpha}$$

Within these two hypotheses, one gets

$$\frac{[\delta_{ind}\Delta E]_{A'} + [\delta_{ind}\Delta E]_{B'}}{2} = \frac{\Delta\mu^2\bar{\alpha}}{2(4\pi\epsilon_0)^2}\int\frac{\rho^2\,d\rho}{\rho^6}\int [1+3\cos(\theta_{0,R})^2]\sin(\theta)\,d\theta\,d\varphi$$

$$|[\delta_{ind}\Delta E]_{A'} - [\delta_{ind}\Delta E]_{B'}| = \frac{|\Delta\mu^2||\Delta\bar{\alpha}|}{2(4\pi\epsilon_0)^2}\int\frac{\rho^2\,d\rho}{\rho^6}\int_\Omega [1+3\cos(\theta_{0,R})^2]\sin(\theta)\,d\theta\,d\varphi \quad (2)$$

Combining these two relationships, one gets

$$\frac{|[\delta_{ind}\Delta E]_{A'} - [\delta_{ind}\Delta E]_{B'}|}{|[\delta_{ind}\Delta E]_{A'} + [\delta_{ind}\Delta E]_{B'}|/2} < \frac{\int_\Omega [1+3\cos(\theta_{0,R})^2]\sin(\theta)\,d\theta\,d\varphi}{\int [1+3\cos(\theta_{0,R})^2]\sin(\theta)\,d\theta\,d\varphi}$$

The two angular integrals depend on the angle between the common direction of μ_1 and μ_0 and the axis of the solid angle Ω and on the half angle delimiting Ω. These values can be derived from the present simulation. One gets an average value of 34° for the first angle and 20° for the second one. It yields

$$\frac{|[\delta_{ind}\Delta E]_{A'} - [\delta_{ind}\Delta E]_{B'}|}{|[\delta_{ind}\Delta E]_{A'} + [\delta_{ind}\Delta E]_{B'}|/2} < 0.045$$

But the effect of induction on the electronic transition energy in the case of retinal in bacteriorhodopsin has been evaluated to be on the order of 0.2 eV.[30] Accordingly, the order of magnitude of the difference between $[\delta_{ind}\Delta E]_{A'}$ and $[\delta_{ind}\Delta E]_{B'}$ (of course not an accurate value) should be $0.045 \times 0.2 = 0.009$ eV. We conclude that the polarization of the protein by the chromophore (induction effect), which was not taken into account in the present calculation, is not likely to account for the two humps (separated by 0.09 eV) of the experimental absorption spectrum of ECFP, although it cannot be neglected in evaluating the energy of the absorption band.

Concerning dispersion in eq 1, it appears that it is a process that is different from induction. In fact, induction can be

completely expressed using the one-electron density, whereas dispersion requires the two-electron density.

One of the key factors contributing to $\delta_{\text{disp}}\Delta E$ (effect of dispersion on the transition energy) is the difference between the dipole polarizabilites of the excited state and the ground state of the chromophore. Here, one finds very similar values (isotropic values): $\alpha_1 = 264.9$ Å^3 and $\alpha_0 = 263.2$ Å^3.

A second factor is the difference between the average transition energies U_0 and U_1. There is no simple way to evaluate such a factor; we may just note that one cannot find nearly equal polarizabilities for the two states if U_0 and U_1 have very different orders of magnitude. Assuming that all three average transition energies U_0, U_1, and U_R have the same order of magnitude $\bar{U} \simeq 0.1$ au, one finds

$$\left(\frac{U_1\alpha_1}{U_1+U_R} - \frac{U_0\alpha_0}{U_0+U_R}\right)U_R \simeq \bar{U}\frac{\alpha_1-\alpha_0}{2} = 0.57 \text{ au}$$

and using the same continuum hypotheses on the polarizabilities as used for induction

$$|\delta_{\text{disp}}\Delta E| = \frac{3}{2}(0.57)\frac{\bar{\alpha}}{(4\pi\epsilon_0)^2}\int\frac{\rho^2\,d\rho}{\rho^6}\int \sin(\theta)\,d\theta\,d\varphi$$

(with everything expressed in atomic units). Then, one gets the difference between conformations A′ and B′ by replacing $\bar{\alpha}$ with $\Delta\bar{\alpha}$ and integrating the angular part inside the solid angle Ω. Then, comparing it with eq 2 leads to the relationship

$$|[\delta_{\text{disp}}\Delta E]_{A'} - [\delta_{\text{disp}}\Delta E]_{B'}| = \Lambda|[\delta_{\text{ind}}\Delta E]_{A'} - [\delta_{\text{ind}}\Delta E]_{B'}|$$

$$\Lambda = \frac{3}{2}(0.57)\frac{2}{\Delta\mu^2}\frac{\int_\Omega \sin(\theta)\,d\theta\,d\varphi}{\int_\Omega [1+3\cos(\theta_{0,R})^2]\sin(\theta)\,d\theta\,d\varphi}$$

The present quantum mechanical calculation yields $\Delta\mu^2 = 10.28$ au, so

$$|[\delta_{\text{disp}}\Delta E]_{A'} - [\delta_{\text{disp}}\Delta E]_{B'}| = 0.050|[\delta_{\text{ind}}\Delta E]_{A'} - [\delta_{\text{ind}}\Delta E]_{B'}|$$

Using the above evaluation $|[\delta_{\text{ind}}\Delta E]_{A'} - [\delta_{\text{ind}}\Delta E]_{B'}| \simeq 0.009$ eV, one gets an order of magnitude of the effect of dispersion on the difference between the transition energies of conformations A′ and B′; it should be on the order of 5×10^{-4} eV.

We conclude that the dispersion effect, not taken into account in the present calculation, is very unlikely to yield a significant contribution to the difference between the absorption spectra of the two conformations of ECFP, in the same way as the induction effect.

Concerning the statistical sampling, an examination of the spectra obtained by taking snapshots only every 10 ps instead of 5ps, that is, 80 snapshots instead of 160, shows that there is no significant difference with the present spectra, and we conclude that the number of snapshots taken into account here is sufficient.

4. Conclusions

In the present work, we have performed molecular dynamics simulations of the two X-ray conformations of ECFP. H-bond networks have been obtained for both conformations. We have pointed out the following results:

- The two conformations are stable along 1 ns trajectories.
- The protein partly quenches the rotation of the chromophore around the two bridging bonds through repulsive van der Waals interactions with a few residues in the chromophore environment.
- The H-bond network in the surroundings of the chromophore differs significantly in the two conformations.

Visible absorption spectra were obtained using quantum mechanical calculations (TDDFT) of the vertical transitions energies of the chromophore in 160 snapshots extracted from the MD trajectories. The main result is that the spectra obtained for the two conformations of the protein are indistinct. This result has been directly related to the dynamic specificities of the two conformations by simple explanatory models supporting the purely numerical result of the TDDFT calculation and thus justifying the use of that method despite its intrinsic limitations. To reach a final interpretation of the experimental spectrum, it would be necessary to examine specific effects that have not be considered here (the partial charge transfer between the chromophore and the residues that are H bonded to it; quantum effects of the internal vibrations of the chromophore; and the difference between the actual protonation state of the protein and the standard protonation considered here). A study of these points is currently in progress.

Acknowledgment. We thank F. Merola for suggesting this study to us and for many fruitful discussions. Thanks are due also to M. Ullmann and E. Bombarda for useful discussions.

References and Notes

(1) Tsien, R. Y. *Annu. Rev. Biochem*. **1998**, *67*, 509−544.
(2) Zimmer, M. *Chem. Rev.* **2002**, *102*, 759−781.
(3) Tozzini, V.; Pellegrini, F.; Beltram, F. In *CRC Handbook of Organic Photochemistry and Photobiology*; Horsphool, W. M., Lenci, F., Eds.; CRC: Washington, DC, 2003; chapter 139.
(4) Morise, H.; Shimomura, O.; Johnson, F. H.; Winant, J. *Biochemistry* **1974**, *13*, 2656−2662.
(5) Palm, G. J.; Zdanov, A.; Gaitaranis, G. A.; Stauber, R.; Pavlakis, G. N.; Wlodawer, A. *Nat. Struct. Biol*. **1997**, *4*, 361.
(6) Chattoraj, M.; King, B. A.; Bublitz, G. U.; Boxer, S. G. *Proc. Natl. Acad. Sci. U.S.A.* **1996**, *93*, 8362.
(7) Lossau, H.; Kummer, A.; Heinecke, R.; Pöllinger-Dammer, F.; Kompa, C.; Bieser, G.; Jonsson, T.; Silva, C. M.; Yang, M. M.; Yoyvan, D. C.; Michel-Beyerle, M. E. *Chem. Phys.* **1996**, *213*, 1.
(8) Cotlet, M.; Hofkens, J.; Michael, M.; Gensch, T.; Van der Auweraer, M.; Michiels, J.; Dirix, G.; Van Guyse, M.; Van der leyden, J.; Visser, A. J. W. G., De Schryver, F. C. *J. Phys. Chem. B* **2001**, *105*, 4999.
(9) Winkler, K.; Linder, J.; Subramaniam, V.; Jovin, T. M.; Wöhringer, P. *Phys. Chem. Chem. Phys*. **2002**, *4*, 1072.
(10) Dickson, R. M.; Cubitt, A. B.; Tsien, R. Y.; Moerner, W. E. *Nature* **1997**, *388*, 355.
(11) Nifosi, R.; Ferrari, A.; Arcangeli, C.; Tozzini, V.; Pellegrini, V.; Beltram, F. *J. Phys. Chem. B* **2003**, *107*, 1679−1684.
(12) Helms, V.; Straatsma, T. P.; McCammon, J. A. *J. Phys. Chem. B* **1999**, *103*, 3263−3269.
(13) Reuter, N.; Lin, H.; Thiel, W. *J. Phys. Chem. B* **2002**, *106*, 6310−6321.
(14) Nifosi, R.; Tozzini, V. *Proteins: Struct., Funct., Genet.* **2003**, *51*, 378−389.
(15) Voityuk, A. A.; Michel-Beyerle, M. E.; Rösch, N. *Chem. Phys. Lett.* **1998**, *296*, 269−276.
(16) Voityuk, A. A.; Michel-Beyerle, M. E.; Rösch, N. *Chem. Phys.* **1998**, *231*, 13−25.
(17) Weber, W.; Helms, V.; McCammon, J. A.; Langhoff, P. W. *Proc. Natl. Acad. Sci. U.S.A.* **1999**, *96*, 6177−6182.
(18) Helms, V.; Winstead, C.; Langhoff, P. W. *J. Mol. Struct: THEOCHEM* **2000**, *506*, 179−189.
(19) El Yazal, J.; Prendergast, F. G.; Shaw, D. E.; Pang, Y. *J. Am. Chem. Soc*. **2000**, *122*, 11411−11415.
(20) Voityuk, A. A.; Kummer, A. D.; Michel-Beyerle, M. E.; Rösch, N. *Chem. Phys*. **2001**, *269*, 83−91.
(21) Chan, M. C.; Lambert, C. R.; Urgitis, J. D.; Zimmer, M. *Chem. Phys*. **2001**, *270*, 157−164.
(22) Tozzini, V.; Nifosi, R. *J. Phys. Chem. B* **2001**, *105*, 5597−5803.

(23) Lill, M. A.; Helms, V. *Proc. Natl. Acad. Sci. U.S.A.* **2002**, *99*, 2778−2781.
(24) Toniolo, A.; Granucci, G.; Martinez, T. J. *J. Phys. Chem. A* **2003**, *107*, 3822−3830.
(25) Marques, M. A. L.; Lopez, X.; Varsano, D.; Castro, A.; Rubio, A. *Phys. Rev. Lett.* **2003**, *90*, 258101.
(26) Laino, T.; Nifosi, R.; Tozzini, V. *Chem. Phys.* **2004**, *298*, 17−28.
(27) Martin, M. A.; Negri, F.; Olivucci, M. *J. Am. Chem. Soc.* **2004**, *126*, 5452−5464.
(28) Zhang, R.; Nguyen, M. T.; Ceulemans, A. *Chem. Phys. Lett.* **2005**, *404*, 250−256.
(29) Warshel, A.; Lappicirella, A. *J. Am. Chem. Soc.* **1981**, *103*, 4664.
(30) Warshel, A.; Chu, Z. T. *J. Phys. Chem. B* **2001**, *105*, 9857.
(31) Callis, P. R.; Liu, T. *J. Phys. Chem. B* **2004**, *108*, 4248.
(32) Spezia, R.; Aschi, M.; Di Nola, A.; Di Valentin, M.; Carbonera, D.; Amadei, A. *Biophys. J.* **2003**, *84*, 2805.
(33) Somers, K. R. F.; Krüger, P.; Bucikiewicz, S.; De Maeyer, M.; Engelborghs, Y.; Ceulemans, A. *Protein Sci.* **2004**, *13*, 1823.
(34) Seifert, M. H. J.; Ksiazek, D.; Azim, M. K.; Smialowsli, P.; Budisa, N.; Holak, T. A. *J. Am. Chem. Soc.* **2002**, *124*, 7932−7942.
(35) Bae, J. H.; Rubini, M.; Jung, G.; Wiegand, G.; Seifert, M. H. J.; Azim, M. K.; Kim, J.; Zumbusch, A.; Holak, T. A.; Moroder, L.; Huber, R.; Budisa, N. *J. Mol. Biol.* **2003**, *328*, 1071−1081.
(36) Villoing, A. *Rapp. DEA* (Université Paris XI) 2003.
(37) Rizzo, M. A.; Springer, G. H.; Granada, B.; Piston, D. W. *Nat. Biotechnol.* **2004**, *22*, 44.
(38) Wang, J.; Cieplak, P.; Kollman, P. A. *J. Comput. Chem.* **2000**, *21*, 1049.
(39) Frisch, M. J.; Trucks, G. W.; Schlegel, H. B.; Scuseria, G. E.; Robb, M. A.; Cheeseman, J. R.; Zakrzewski, V. G.; Montgomery, J. A., Jr.; Stratmann, R. E.; Burant, J. C.; Dapprich, S.; Millam, J. M.; Daniels, A. D.; Kudin, K. N.; Strain, M. C.; Farkas, O.; Tomasi, J.; Barone, V.; Cossi, M.; Cammi, R.; Mennucci, B.; Pomelli, C.; Adamo, C.; Clifford, S.; Ochterski, J.; Petersson, G. A.; Ayala, P. Y.; Cui, Q.; Morokuma, K.; Malick, D. K.; Rabuck, A. D.; Raghavachari, K.; Foresman, J. B.; Cioslowski, J.; Ortiz, J. V.; Stefanov, B. B.; Liu, G.; Liashenko, A.; Piskorz, P.; Komaromi, I.; Gomperts, R.; Martin, R. L.; Fox, D. J.; Keith, T.; Al-Laham, M. A.; Peng, C. Y.; Nanayakkara, A.; Gonzalez, C.; Challacombe, M.; Gill, P. M. W.; Johnson, B. G.; Chen, W.; Wong, M. W.; Andres, J. L.; Head-Gordon, M.; Replogle, E. S.; Pople, J. A. *Gaussian 98*, revision A.6; Gaussian, Inc.: Pittsburgh, PA, 1998.
(40) Ridard, J.; Lévy, B. *J. Comput. Chem.* **1999**, *20*, 473.
(41) Case, D. A.; Pearlman, D. A.; Caldwell, J. W.; Cheatham, T. E., III; Wang, J.; Ross, W. S.; Simmerling, C. L.; Darden, T. A.; Merz, K. M.; Stanton, R. V.; Cheng, A. L.; Vincent, J. J.; Crowley, M.; Tsui, V.; Gohlke, H.; Radmer, R. J.; Duan, Y.; Pitera, J.; Massova, I.; Seibel, G. L.; Singh, U. C.; Weiner, P. K.; Kollman, P. A. *AMBER 7*; University of California: San Francisco, CA, 2002.
(42) Darden, T.; York, D.; Pedersen, L. *J. Chem. Phys.* **1993**, 98, 10089.
(43) Sham, Y. Y.; Warshel, A. *J. Chem. Phys.* **1998**, *109*, 7940.
(44) Nam, K.; Gao, J.; York, D. M. *J. Chem. Theory Comput.* **2005**, *1*, 2.
(45) Luzkhov, V.; Warshel, A. *J. Am. Chem. Soc.* **1991**, *113*, 4491.
(46) Wanko, M.; Hoffmann, M.; Strodel, P.; Koslowski, A.; Thiel, W.; Neese, F.; Frauenheim, T.; Elstner, M. *J. Phys. Chem. B* **200**5, *109*, 3606.
(47) Fantacci, S.; Migani, A.; Olivucci, M. *J. Phys. Chem. A* **2004**, *108*, 1208−1213.
(48) Stone, A. J. *The Theory of Intermolecular Forces*; Clarendon Press: Oxford, England, 1996.